International Journal of Concrete Structures and Materials

RESEARCH Open Access

Structural Performance of Flexural and Shear-Deficient Pre-cracked Reinforced Concrete Beams Retrofitted with Knitted Glass Fabric-Reinforced Cementitious Matrix

R. Kirthiga[1] and S. Elavenil[1*]

Abstract

This study investigates the retrofitting of concrete structures to restore and enhance the load capacity of deteriorated structural members using external strengthening techniques. The novelty of the study is the use of agro-industrial waste as a binder for fiber-reinforced polymer (FRP) sheets. Experimental testing and finite-element analysis (FEA) are performed to evaluate the effect of glass fabric-reinforced cementitious matrix (GFRCM) on the flexural and shear deficiencies of pre-cracked, retrofitted reinforced concrete (RC) beams. ANSYS software is used for FEA to analyze the load–deflection behaviour of the retrofitted RC beam, facilitating a comparison with experimental results. The results indicated significant enhancements in structural performance, with load-carrying capacity increases between 2% and 32%, and deflection ranging from 4% to 22%. These improvements in load-carrying capacity are attributed to the use of double layers of GFRCM, which effectively improves the load-carrying capacity and overall performance. The FEA predictions aligned well with the experimental findings, confirming that increasing the number of GFRCM layers significantly enhance the structural capacity of retrofitted RC beams.

Highlights

- GFRCM improves flexure and shear in pre-cracked RC beams.
- FE analysis predicts the load–deflection behaviour of RC beams.
- Retrofitted beams enhance load-carrying capacity and reduce beam deflection.

Keywords Deteriorated structural members, Glass fabric-reinforced cementitious matrix, Finite-element analysis, Fiber reinforced polymer, ANSYS, Load-carrying capacity, Deflection

1 Introduction

In recent years, the demand for rehabilitating deteriorated concrete structures has increased significantly (Kalyani & Pannirselvam, 2023). Fiber-reinforced polymers (FRP) have been widely adopted as externally bonded reinforcements for deficient structural members due to their high strength-to-weight ratio, corrosion resistance, ease of application, and minimal impact on

*Correspondence:
S. Elavenil
elavenil.s@vit.ac.in
[1] School of Civil Engineering, Vellore Institute of Technology, Chennai Campus, Chennai 600127, India

structural geometry (Kirthiga & Elavenil, 2022). However, FRP systems relying on epoxy resins face challenges, including poor thermal resistance, high cost, incompatibility with moist surfaces, and limited bonding with concrete substrates (Natraj et al., 2023). These challenges can be lessened by cement-based mortars (Kirthiga & Elavenil, 2023). Yet, the high fineness of cement mortars can hinder fiber impregnation and bonding. Replacing fiber sheets with fabric textiles enhances the fiber–matrix interaction (ACI Committee 549.4R-13, 2013), as these fabrics consist of fiber rovings arranged in mesh form (Koutas et al., 2019). Therefore, embedding high-strength fabric meshes into cementitious mortars leads to the development of fabric-reinforced cementitious matrix (FRCM) systems (FRCM) (Elsanadedy et al., 2019), which offer improved compatibility with concrete, thermal resistance, and ease of installation (Aljazaeri & Myers, 2016; Donnini et al., 2017; Ebead & Younis, 2019; Yin et al., 2016). The mechanical performance of FRCM composite is significantly influenced by the properties of both the fabric and cement matrix (Kirthiga & Elavenil, 2024; Sagare et al., 2024).

FRCM is effective for strengthening various RC elements, such as beams, columns, slabs, and masonry walls (Donnini et al., 2016a; Kirthiga & Elavenil, 2022). This technique involves externally bonding unidirectional sheets impregnated with cement or polymer-based binders (Tzoura & Triantafillou, 2016). The performance of FRCM is closely tied to the bond quality between the fabric and mortar matrix, which can be enhanced by incorporating short fibers (Donnini et al., 2016b; Zhang & Deng, 2022). Adding short carbon and AR-glass fibers significantly improves tensile strength (Barhum & Mechtcherine, 2012), while polyvinyl alcohol fibers shift the failure mode from fabric slippage to rupture, enhancing the performance of GFRCM (Song et al., 2023). Numerous studies using experimental, analytical, and numerical approaches have examined the behavior of FRCM-retrofitted RC beams. The RC beam retrofitted with PBO and carbon–FRCM increased its flexural capacity to 54% and attained fabric slippage failure (D'Ambrisi & Focacci, 2011). PBO–FRCM exhibited greater ductility than carbon–FRCM, with failure modes influenced by the number of fabric layers (Ebead et al., 2017). Increasing the number of layers improved the load capacity by 77% but reduced ductility (Ombres, 2011). Mohan et al. found that RC beams strengthened with basalt and glass fabrics using cementitious binders outperformed those using geopolymer mortars in flexural strength. Beam retrofitted with four layers exhibited the highest increase in ultimate load of about 42.06%, compared to those with two and six layers (Mohan and Madhavi, 2024). Increasing the number of layers enhanced beam stiffness and altered the failure mode from concrete crushing to fabric slippage within the matrix (Ebead et al., 2017; El-Maaddawy & El Refai, 2016; El-Sherif et al., 2020). Aljazaeri et al. observed a 21% improvement in load capacity for RC beams retrofitted with U-wrapped glass–FRCM compared to unstrengthened beams (Aljazaeri & Myers, 2016). The U-shaped glass fabric configuration also led to significant increases in both load capacity and mid-span deflection (Aljazaeri & Myers, 2016; Zeng et al., 2017). Wakjira and Ebead (2018) reported that the shear strengthening with carbon–FRCM improved shear capacity by 43–114%. Similarly, Ramezani and Esfahani (2023) noted an increase in shear capacity from 21.3% to 23.1% using carbon fabric, compared to traditional FRP systems. Yang et al. reported notable shear capacity enhancements ranging from 50.9% to 160.6%, despite debonding failure in the strengthened layers (Yang et al., 2020). The addition of polyvinyl alcohol fibers has been shown to improve the toughness and durability of FRCM, contributing to long-term performance (Dong et al., 2020; Guo et al., 2022). Azam et al. reported that shear-strengthened beams reached up to 105% shear capacity, although they found little difference between side-bonded and U-wrap configurations (Azam et al., 2018). Tetta et al. revealed that U-wrapping outperformed side-bonded configuration, resulting in significantly higher shear strength (Tetta et al., 2016).

Many researchers prefer finite-element modeling (FEM) to study the behavior of structural components strengthened with FRCM, since experimental testing is time-consuming and requires extensive resources (Talaat et al., 2022). A critical aspect of FEM analysis is accurately capturing the interaction between the concrete substrate and the external strengthening layer (Revanna & Moy, 2023). Debonding or rupture failures generally arise from inadequate bonding either between the concrete surface and the retrofitting material or within the internal layers of the FRCM system. Cohesive contact laws clearly define the fabric to mortar interaction (Mercedes et al., 2021). Ombres and Verre (2021) modeled RC beams retrofitted with steel-reinforced grout for both flexure and shear strengthening. A parametric analysis revealed the impact of a composite thickness on structural response, emphasizing the importance of phenomenological model in understanding damage mechanisms (Truong et al., 2016). The matrix and concrete interface was simulated using cohesive contact and traction separation laws. However, the FEM under predicted the load capacity by around 5% compared to experimental values (Ombres & Verre, 2019). Revanna et al. modelled and validated a FEM using experimental data, achieving variance of 6.02% for ultimate load and 5.7% for deflection, then extended it to investigate debonding behaviour possible

preventative strategies (Revanna & Moy, 2023). Katsamakas et al. analyzed shear-strengthening beams and found deviations of approximately 1% in load, 10% in displacement, and 4.2% in energy absorption compared to experimental results (Katsamakas et al., 2021). Basalt fabric was used as an external jacket to strengthen the concrete cylinders with engineered cementitious composites, and it was found that the experimental results closely matched the numerical results. Hao et al. observed that FEM could predict maximum loads between 46% and 57%, and cracking loads between 3% and 35% for beams retrofitted with galvanized steel mesh (Hao et al., 2022). Chen et al. confirmed close agreement between numerical and experimental results for concrete cylinders strengthened with basalt fabric (Chen et al., 2023). Grande and Milani developed a numerical model to investigate the progressive damage in the outer mortar layer, which affects stress transfer between fabric and mortar. Their spring-based model incorporated various retrofitting components with both linear and non-linear properties (Grande & Milani, 2018). Sucharda conducted a non-linear fracture plasticity model to predict failure modes and load-carrying capacity in FRCM-retrofitted beams (Sucharda, 2020). Mercedes et al. simulated RC beams strengthened with different FRCM. The moment–deflection curves indicated that steel fabric provided the highest strength gain (78%), followed by PBO (6%), while basalt and carbon fabrics exhibited inconsistent effects (Mercedes et al., 2021). Numerous numerical studies have been conducted, but a significant gap remains in accurately predicting the behaviour of RC beams, highlighting the need for more focused research in this area.

In this study, the behavior of pre-damaged RC beams retrofitted with AR-glass FRCM is investigated under four-point bending until failure. The experimental findings are compared with a finite-element model developed in ANSYS, capturing the beam's nonlinear response. The validated model is also used to explore the effects of debonding and evaluate performance under similar retrofitting configurations.

2 Materials and Methods

2.1 Material Properties

For casting RC beams, the concrete mix consists of ordinary Portland cement, river sand, and gravel with sizes varying from 12 to 20 mm. The cement was purchased from Chettinad Cement Co. Ltd., Chennai, India, while the river sand and gravel were purchased from the local vendors. A water–cement ratio of 0.35 was adopted. The compressive strength of the concrete was measured according to IS 516 (Part 1/Sec1):2021. Three concrete cubes measuring 150 mm×150 mm×150 mm were casted and tested. After 28 days of curing, the average compressive strength was found to be 38.25 MPa with a coefficient of variation of 2.35%. The manufacturer reported the yield strength of the reinforcement steel bars to be 500 MPa.

This study uses bi-directional Alkali Resistance (AR) glass fabric mesh as a retrofitting material due to its temperature resistance in cementitious matrices. The AR-glass fabric was sourced from Covai Seenu and Company, in Coimbatore, Tamil Nadu, India. This fabric is made of knitted glass with a mesh size 3×3 mm in both directions. It has a cross-sectional area of 1.4 mm^2, weighs 125 g/m^2, and has a thickness of 0.0035 mm. A tensile test was conducted on the single yarns to examine the tensile properties using a 50 kN tensile testing machine at a 0.5 mm/min speed. Figure 2 shows the tensile testing of glass fabric strip and yarns in both direction. The tensile strength of fabric strip, yarn in the warp and weft direction were calculated as 1121 MPa, 1233 MPa, and 1120 MPa, respectively, with co.efficient of variations of 12.62%, 8.11%, and 14.28%. Figure 1 shows the image of glass fabric sheet and Fig. 2a shows tensile test on glass fabric strip, (b) tensile test on the yarn in the warp direction, and (c) tensile test on the yarn in the weft direction.

Sugar refineries crush sugarcane stalks to extract juice, and the leftover residue is burned to produce bagasse ash. Bagasse ash contains a high amount of amorphous silica, which improves the strength property. Bagasse ash was obtained from Kothari Sugars and chemicals Ltd. in the Ariyalur district of Tamilnadu, India. The bagasse ash dried in an oven for 24 h and then sieved to a particle size of 75 µm. Silica fume is a byproduct from the silicon and ferrosilicon industries during the smelting process of silicon metal or ferrosilicon alloys. Silica fume was sourced from the Astra Chemicals, Chennai, India. Table 1 shows the physical properties of cement, silica fume, and

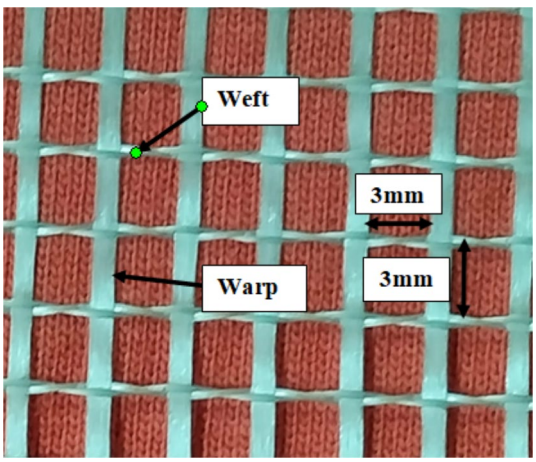

Fig. 1 Image of AR-glass fabric sheet

(a) (b) (c)

Fig. 2 **a** Tensile test on glass fabric strip. **b** Tensile test on the yarn in the warp direction. **c** Tensile test on the yarn in the weft direction

Table 1 Physical properties of cement, SF, SCBA and sand

Physical properties	OPC	SF	SCBA	Sand
Specific gravity	3.14	2.2	2.67	2.65
Initial setting time (min)	75	–	–	–
Final setting time (min)	365	–	–	–
Surface Area (m^2/g)	3.360	3.8641	25.59	–
Water absorption (%)	–	–	–	0.1
Fineness (%)	5	–	–	–
Particle size	–	1 µm	–	< 150 mm

bagasse ash. The chemical compositions of raw material are given in Table 2. The X-ray fluorescence technique was carried out to assess the chemical composition of material, such as cement, SF and SCBA. It was observed that 75.98% of SCBA was made up of silica oxide, and that its LOI is 7.8, which conforms to the criteria and can be used as an SCM. The composition of Al_2O_3, Fe_2O_3 and CaO are found to be incredibly low. Similarly, SF also has significant silica content of about 98.6%, which enhances the pozzolanic property.

The binder prepared for FRCM is composed of cement, bagasse ash, silica fume, very fine sand, polyvinyl alcohol (PVA) fibers and additives. A fine aggregate were selected to be smaller than 150µ. The PVA fibers measures 6 mm in length and 24 mm in diameter. Polycarboxylates ether-based superplasticizer was used to improve the workability. To identify the optimum mix proportions, mortar cubes were tested as per IS: 14,858:2000, and these test results were published in the study conducted by Kirthiga et al. (Kirthiga & Elavenil, 2023). The compressive, flexural, and split-tensile strength were determined as 63 MPa, 10.15 MPa, and 4.2 MPa with variations of 25.39%, 18.92%, and 15.4%. Table 3 presents the optimum mix proportions of cement binders, expressed as weight percentage of the binder.

2.2 Beam Specification

The RC beams, measuring 1500 mm in length, 100 mm in width, and 150 mm in depth are grouped into flexure- and shear-deficient beams. The RC beams were intentionally pre-cracked to 50%, 75%, and 100% of their ultimate load capacity. These damage levels were defined based on the percentage of the peak load recorded from an unstrengthened control beam. To induce the desired damage levels, each beam was loaded up to the corresponding percentage of this ultimate load. The extent of damage

Table 2 Chemical composition of OPC, SF and SCBA

Composition (%)	SiO_2	Fe_2O_3	Al_2O_3	Mno	CaO	Mgo	Na_2O	K_2O	SO_3	P_2O_5	TiO_2
OPC	21.12	3.2	5.2	–	65.4	1.2	0.12	0.73	2.3	–	–
SF	98.6	0.037	0.49	–	0.17	0.032	0.028	0.37	0.25	0.014	0.006
SCBA	75.98	2.37	3.71	0.081	4.86	2.05	0.38	2.6	–	1.91	0.3

Table 3 Mix proportion of cement binder

Cement	Bagasse ash	Silica fume	Fine sand	Water reducer	PVA	Water
1	0.10	0.10	0.8	0.2	0.0045	0.35

was verified through visual observation of crack patterns and measurement of deflection prior to the retrofitting process. This approach ensured consistent and controlled pre-cracking conditions for all retrofitted specimens. Reinforcement bars with 10 mm and 12 mm were used as main reinforcement, while a bar with 8 mm diameter was used as transverse reinforcement. To design a deficient beam, the area of steel in the tension zone is reduced for flexural-deficient beams, while for shear beams, the area of shear reinforcement is reduced, typically achieved by increasing the spacing of the stirrups.

The control beam is reinforced with two 12 mm diameter bars in both tension and compression zones, and 8 mm diameter bars are used as stirrups, placed at 100 mm center-to-center (c/c) spacing. The flexural and shear-deficient beam consists of six beams, pre-cracked to 50%, 75%, and 100% and retrofitted with one and two layers of GFRCM. The flexural-deficient beams are designed with two 10 mm bars in the tension zone to intentionally induce flexural failure. For shear-deficient beams, the stirrups are placed at 300 mm spacing c/c to induce shear failure. The grade of the steel used for the reinforcement bar is Fe500. The reinforcement details, damage level, and strengthening layers are shown in Table 4. In this study, the notation used for the specimens is as follows: FF represents flexural-deficient beams, while SF denotes shear-deficient beams, the number 50, 75, and 100 indicates the damage level in percentage (%), and 1 and 2 represents the number of strengthening layers applied.

2.3 Test Setup and Application Process of GFRCM

Figure 3a illustrates the experimental setup used for testing the specimens. All beams, with an effective span of 1.2 m, were subjected to two-point loading applied transversely at one-third of the span length from each support. A testing machine applied a central point load, which was distributed into two equal loads using spreader beams. The mid-span displacement was recorded using a dial gauge mounted at the soffit of each beam. Steel plates were placed at the loading and support points to ensure safe and effective load transfer. The control beam (CB) was loaded until failure, while the other beams were pre-loaded to different damage levels. These pre-loaded beams were then repaired using a cement-based binder and cured for 3 days. Afterward, they were retrofitted with GFRCM and cured for an additional 7 days before being reloaded to failure.

The U-shaped configuration was applied to the pre-cracked beams using a systematic process. The U-shaped covered the bottom soffit and both side faces of the RC beams. This process starts with preparing the concrete surface through scouring, sandblasting, and moistening the substrate to enhance the bonding among the matrix and the concrete substrate. A 2 mm thick cement binder was then applied to the moistened concrete substrate and then AR-glass fabric mesh was carefully embedded into the cement binder. Finally, a second binder layer was applied to encapsulate the fabric completely.

For the flexure-deficient beam, GFRCM was applied over a 900 mm length at the midspan and across the full width of 400 mm, with a 2 mm thick layer of cementitious binder, as shown in Fig. 3b. This application is positioned in the areas experiencing maximum bending moments to improve flexural strength and stiffness. For the shear-deficient beam, GFRCM was positioned near both ends of the beam supports, specifically under the shear zones, as shown in Fig. 3c.

Table 4 Reinforcement details for retrofitted beams

Group Name	Model ID	Damage level (%)	Strengthening layer	Bottom Reinforcement	Top Reinforcement	Stirrups
Control	CB	100	–	2-Ø12mm	2-Ø12mm	Ø8mm@100 mm
A	FF-50–1	50	1	2-Ø10mm	2-Ø12mm	Ø8mm@100 mm
	FF-50–2		2			
	FF-75–1	75	1	2-Ø10mm	2-Ø12mm	Ø8mm@100 mm
	FF-75–2		2			
	FF-100–1	100	1	2-Ø10mm	2-Ø12mm	Ø8mm@100 mm
	FF-100–2		2			
B	SF-50–1	50	1	2-Ø12mm	2-Ø12mm	Ø8mm@300 mm
	SF-50–2		2			
	SF-75–1	75	1	2-Ø12mm	2-Ø12mm	Ø8mm@300 mm
	SF-75–2		2			
	SF-100–1	100	1	2-Ø12mm	2-Ø12mm	Ø8mm@300 mm
	SF-100–2		2			

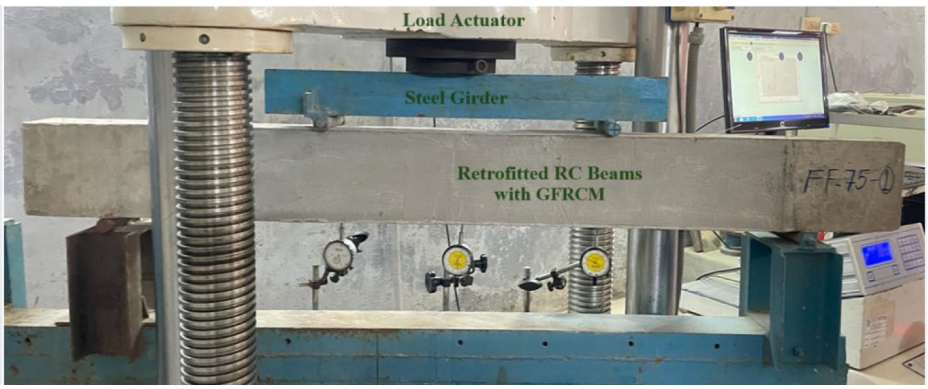

(a)

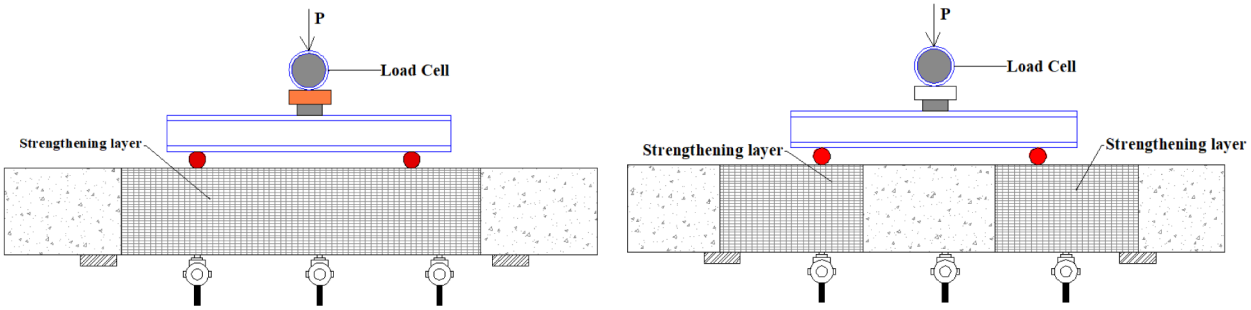

(b) (c)

Fig. 3 **a** Test setup. **b** Flexure deficient retrofitted beam. **c** Shear-deficient retrofitted beam

Each strengthening layer was applied over a 400 mm length and covered the full width of 400 mm, with 2 mm thick layer of cementitious binder, as shown in Fig. 3c.

3 Finite-Element Analysis

Finite-element analysis (FEA) analysis enables a more efficient simulation of the non-linear behavior of RC members with a high degree of accuracy within a shorter duration (Hassan et al., 2017). In FEA, the structure is depicted as an assembly of finite elements, each possessing distinct material properties, collectively influencing the determination of the structure's overall behavior (Mahmoud, 2016). In this study, ANSYS 2024 R2 software is used to model the RC-strengthened beams and compared with the experimental results. Discrete reinforcement models are utilized to represent the reinforcement bars embedded in the concrete.

3.1 Modelling of Concrete, Reinforcement Bars and Steel Plates and Its Properties

The SOLID 186 element is shown in Fig. 4a, used to model the concrete, and effectively manage the nonlinear behavior during tension and compression, including the occurrence of crushing under compression. It is characterized by 8 nodes, each with 3 degrees of freedom (DOF), and its essential feature of this element lies in its handling of nonlinear material properties. Concrete exhibits non-linear behaviour owing to its quasi-fragility. The plasticity hardening behavior of concrete under compression is derived from the Menetrey-Willam theory and uses a non-associated flow rule of the Drucker-Prager type. REINF 264 element is shown in Fig. 4b, is used to determine the inherent stresses and strain for the reinforcement steel bar and ensures their exact positions. This component is suitable for modelling the cables, springs, trusses, links, etc. These elements are specified by two nodes, with the section type and the material properties. It functions as compression–tension uniaxial

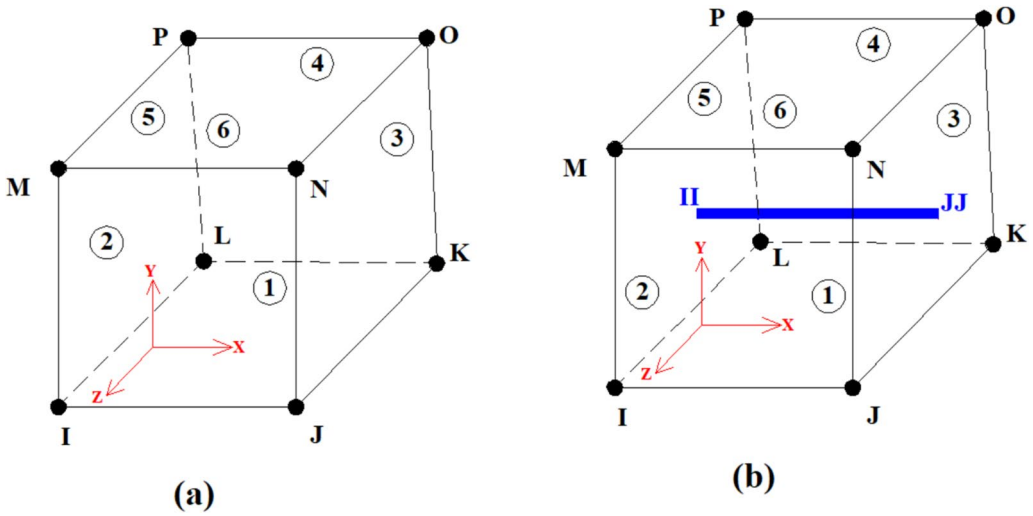

Fig. 4 **a** SOLID186. **b** REINF 264

Table 5 Concrete and steel material properties used in FE modelling

Material	Property	Value
Concrete	Young's modulus (MPa)	31,425
	Poisson ratio	0.15
	Menetrey-Willam	
	Uniaxial Compressive strength (MPa)	38.5
	Uniaxial Tensile strength (MPa)	3.59
	Biaxial Compression strength (MPa)	30
	Dilatancy angle (Degree)	30
	Plastic strain at uniaxial compression strength	0.001
	Plastic strain at transition from Power Law to Exponential softening	0.002
	Relative stress at start of non-linear Hardening	0.3
Steel	Young's modulus (GPa)	210
	Poisson ratio	0.3
	Yield strength (MPa)	500

elements with 3DOF that can withstand considerable deflection under loading. Table 5 shows the concrete and steel material properties used in FE modelling. SOLID186 elements are utilized to replicate the steel plates supporting the RC beam and the applied loads. This element has 20 nodes, with 3 DOF in all directions. SOLID186 is an advanced 3D solid element with quadratic displacement behavior. This element supports plasticity, deflection, strain, creep, stiffening, etc. The reinforcement bars and plates used in the FE models were designed to be flexible components that exhibit linear behaviour with elastic modulus of 210 GPa and Poisson's ratio of 0.3. The yield stress varies based on the element used.

3.2 Cement Binder and AR-Glass Fabric: Modeling and Its Properties

The cement binder is similarly modelled with SOLID 181 element, as shown in Fig. 5a. SHELL181, a three-dimensional layered solid element, is used to model the glass fabric added to reinforce the RC beams. Surface-to-surface contact pairs were utilized at the interaction with the concrete substrate and the GFRCM. The concrete surface was modelled using TARGE170, and the GFRCM was modelled using CONTA173 (Jawdhari et al., 2020), as shown in Fig. 5b. The fabric and cement binder are stimulated as a single element with multiple layers. TARGE170 has the ability to signify the 3D target surfaces for the corresponding contact elements. CONTA173 is utilized to denote the interaction and movement between the 3D target surface and also with a deformable surface. Table.6 provides the properties of cement binder and glass fabric sheet.

The interaction between hardening and damage variables governs the development of damage and the concrete soften behavior. These variables affect the concrete stress–strain curve's post-yielding region, specifically occurring after the material has exceeded its elastic limit. These values are usually obtained by static testing. ANSYS used the values proposed by Zreid and Kaliske for the compression damage evolution, hardening parameter, and threshold value (Zreid & Kaliske, 2018). The tension damage value was set to zero, assuming that concrete begins to soften in tension as soon as the elastic limit is reached (Si Larbi et al., 2013). To include the debonding characteristics in the FE model, the interface between the concrete and GFRCM was identified as the weakest layer and is simulated using cohesive zone material and

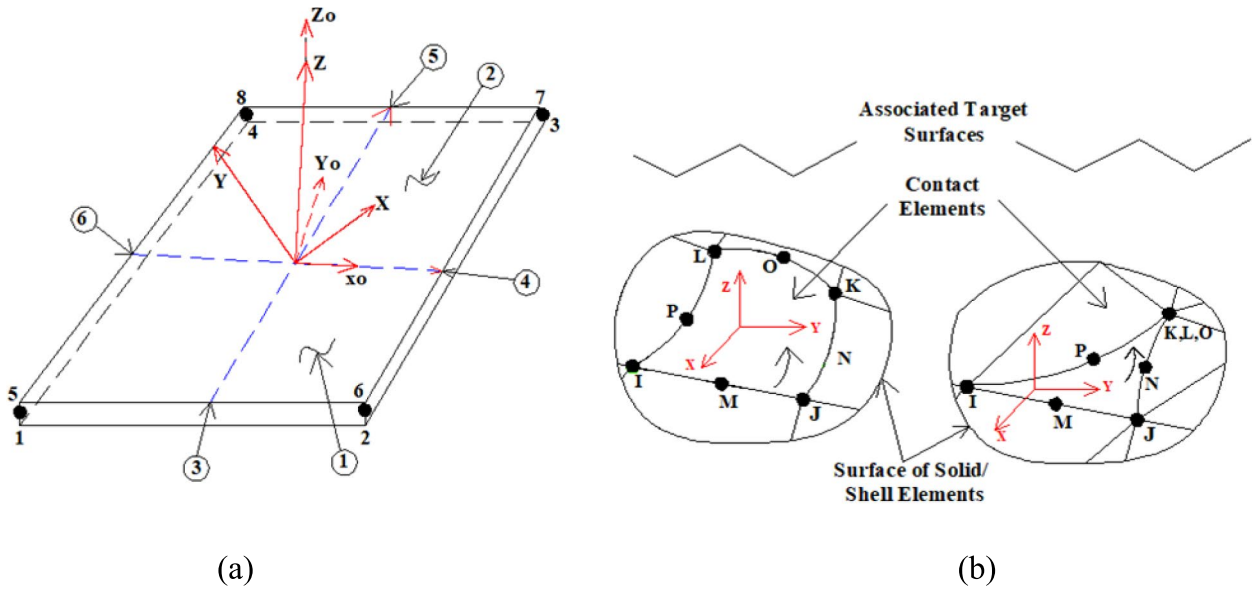

Fig. 5 **a** SHELL181. **b** CONTA173

Table 6 GFRP and cement binder properties

Material	Property	Value
GFRP	Young's modulus (MPa)	74,000
	Poisson's ratio	0.18
	Layer Thickness (mm)	0.036
	Number of layer	1,2
Cement binder	Young's modulus (MPa)	25,500
	Tensile strength (MPa)	2.2
	Poisson's ratio	0.23
	Layer Thickness (mm)	2
	Number of layer	1,2,3

contact pairs. Debonding in most studies was examined by analyzing the shear stress-slip behaviour of the interfaces (Omran & El-Hacha, 2012).

3.3 Meshing and Boundary Conditions

The support and loading plates were modelled to align perfectly with the concrete beam. The modelled beams use a mesh with 15 mm square size elements, as specified by sensitivity study. Notably, Al-Huri et al. (2022) and (Wei et al., 2025) both employed a 15 mm mesh size in their simulations of strengthened or hybrid RC beams. Their results demonstrated that this mesh size provides a good balance between computational efficiency and accurate prediction of structural behavior, validating its use for modeling GFRCM-retrofitted beams in this study. The element size is chosen to balance the precision of results with the time required for the cost analysis. Displacement boundary conditions are necessary to constrain the model and obtain a notable solution. Boundary conditions are applied to the supports to guarantee the model acts like the tested beam. In this study, one support will be modelled as a pin, restricting movement in all directions, while the other support will be modelled as a roller, allowing movement only in the Z direction. Figure 6 displays the finite-element models and meshing of control and retrofitted beams with boundary conditions.

A static analysis with large displacement was performed to identify the non-linearity. A vertical displacement was applied to the upper plate in displacement-controlled analysis to replicate the forces observed in the experimental test. Displacement was incrementally applied, and the processes were segmented into several series of load steps. The activation of time stepping manages the step size and ensured

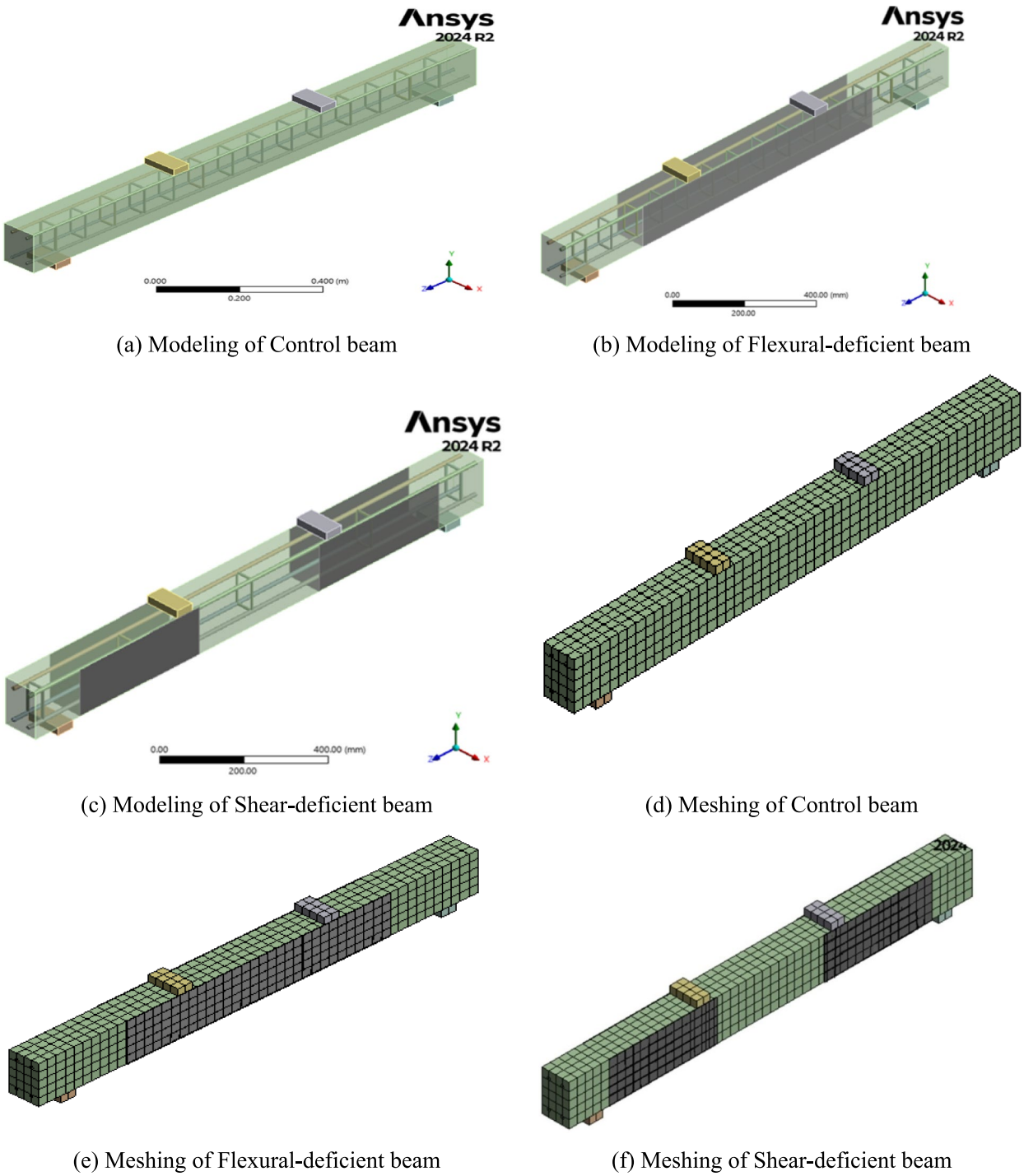

(a) Modeling of Control beam

(b) Modeling of Flexural-deficient beam

(c) Modeling of Shear-deficient beam

(d) Meshing of Control beam

(e) Meshing of Flexural-deficient beam

(f) Meshing of Shear-deficient beam

Fig. 6 Modeling and meshing of control and retrofitted beam with GFRCM

convergence in the solution. The convergence criteria for analysis were defined by displacement and force, with tolerance of 0.1% and 0.5%. The interaction modelling impacts the failure pattern in the strengthened beam.

FRCM strengthening generally involves four possible failure modes. One of these is concrete crushing, which prevents the use of fabrics and reinforcing bars. The second mode is fabric rupture, which occurs when the yarn filaments reach their maximum elongation capacity. The

third mode is steel yielding, which occurs before either the fabrics rupture or the concrete crushes. Finally, failure may also result from debonding of the FRCM layer from the concrete substrate.

3.4 Parametric Investigation on Strengthening of Flexural- and Shear-Deficient Beams

The effects of strengthening deficient beams are investigated using FE models. GFRCM was applied in a U-wrap configuration to retrofit the deficient beam in both flexure and shear zones. The FE modelling of the retrofitted RC beam involves a layer-by-layer representation of GFRCM. The model includes the volume of the cement binder and the glass fabric mesh in the flexure and shear zones. The glass fabric mesh is modelled with a thickness of 0.036 mm, and the cement binder is modelled with a thickness of 2 mm. Element types, material properties, and constants are assigned accordingly. Cohesive zone material modeling is utilized and FEA is performed to assess the strengthening effects. Figure 7 represents the modeling of glass fabric layers and cement binder,

4 Results and Discussion

4.1 Flexural-Deficient Beams Strengthened with GFRCM

The CB failed at a maximum load of 61.35 kN due to the yielding of steel reinforcement and the concrete crushing in the compression zone. All the retrofitted beams had a substantially higher load-carrying capacity than control beam. Specimens FF-50–1, FF-75–1, and FF-100–1, retrofitted with one layer, achieved maximum load of 78.69 kN, 72.53 kN and 63.42 kN, respectively, with mid-span deflection of 13.47 mm, 12.09 mm, and 12.54 mm. The specimens FF-50–2, FF-75–2, and FF-100–2, retrofitted with two layers, attained maximum loads of 86.59 kN, 77.12 kN, and 68.37 kN with deflection of 11.41 mm, 11.3 mm, and 12.88 mm.

The load–deflection curve for a strengthened RC beam typically shows three phases. The initial phase is elastic, with minimal cracking and a linear curve response. In the second phase, the curve becomes non-linear and a cracks develop in both the concrete and FRCM, causing the beam to deform more quickly under load. The final phase signifies ultimate failure, characterized by crack propagation, which leads to an increase in deflection and a significant reduction in load-carrying capacity. This progression highlights the beams behavior and the effectiveness of the FRCM strengthening. After reaching their peak load, all retrofitted beams displayed similar behavior.

4.1.1 Comparison of FEA Result with Experiment Result

Table 7 summarizes the load-carrying capacity and deflection of the retrofitted beams attained from numerically and experimentally. In addition, Table 7 includes the ratio of FE to experimental load-carrying capacity and displacements of the retrofitted beams. The FEA and experimental results are correlated graphically in Fig. 8. The flexural capacity of the retrofitted beam varies from

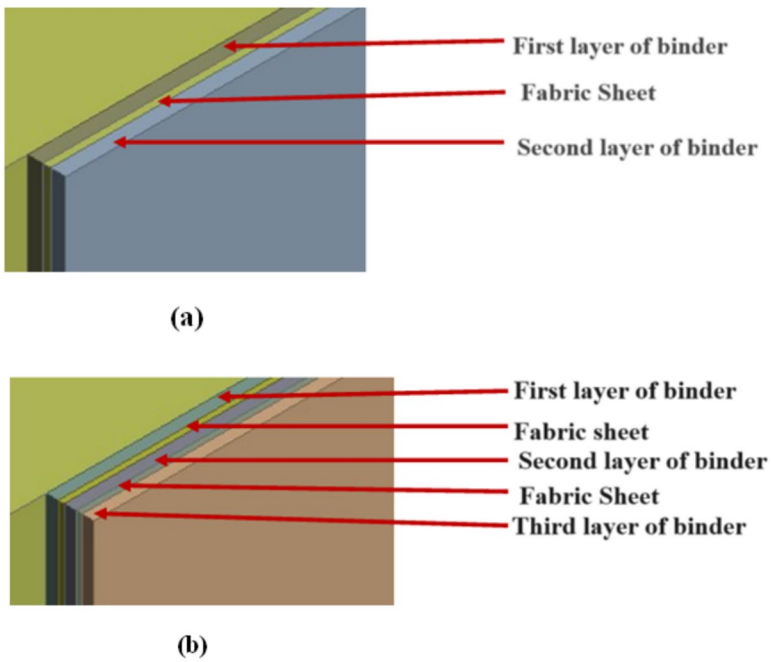

Fig. 7 Modelling of GFRP and Cement binder (**a**) single layer, (**b**) double layer

Table 7 Load-carrying capacity and deflection of the flexural-deficient retrofitted beam

Specimens	No. of layers	FEA		Experiment		P_A/P_E	δ_A/δ_E	Failure modes (Exp)
		Max. Load P_A (kN)	Deflection, δ_A (mm)	Max. Load, P_E (kN)	Deflection, δ_E (mm)			
CB	–	64.565	15.14	61.2	14.12	0.95	0.93	Flexure
FF-50%-1	1	79.906	13.728	78.69	13.49	0.98	0.98	Flexure + Delamination
FF-50%-2	2	85.263	11.637	86.587	11.41	1.02	0.98	Flexure + Debonding
FF-75%-1	1	72.853	12.091	72.532	12.1	1.00	1.00	Delamination
FF-75%-2	2	73.774	11.594	77.122	11.03	1.05	0.95	Delamination
FF-100%-1	1	65.964	11.94	63.416	12.54	0.96	1.05	Fabric rupture
FF-100%-2	2	68.256	11.36	68.366	11.39	1.00	1.00	Fabric slippage

0.95 to 1.05 with a correlation of 0.954, while the deflection ranges from 0.93 to 1.05 with correlation of 0.882. The load–deflection curves from both experimental and FE analysis are closely matched, reflecting a strong agreement for all beams. Sivasuriyan et al. (2024) performed two-point loading tests on RC beams and evaluated the results using FEA in ANSYS. The numerical analysis closely matched the experimental outcomes in terms of both load capacity and deflection. This strong correlation validated the effectiveness of the FEA model in capturing the flexural response of RC beams. The study by Sasikumar et al. confirmed that the FE model exhibited strong correlation with experimental results, effectively representing the flexural performance of damaged RC members (Sasikumar & Candassamy, 2024). This agreement with experimental results boosts its reliability for predicting the performance of retrofitted RC beams in real-world scenarios.

4.1.2 Load–Deflection Curve

The numerical analysis predicted an ultimate load of 64.57 kN for the CB, while the experimental results recorded a maximum load of 61.2 kN. The strengthened beam with flexural deficiency specimens exhibited a much higher flexural failure load compared to the control beam. Figure 9 presents a comparison between the load–displacement curves obtained from FE simulation and experimental tests for the retrofitted beam. All retrofitted beams displayed nearly identical behaviour after reaching the ultimate load and showed a significant increase in deflection under a sustained residual load. When a load increases, the retrofitted beam reaches its cracking point, resulting in reduced stiffness and changed to nonlinear behavior. At this phase, the concrete in tension cracks and the load is carried by the external strengthening layer GFRM, indicating that the beam is approaching its load capacity. After reaching the ultimate load, the beam reaches its maximum strength. However, beyond this point, the graph shows a reduction in load, reflecting post-behaviour, indicating that the beam carrying capacity has been reduced. This post-yielding phase continued until fabric rupture resulted in the loss of strengthening effect, and a failure mode was observed by Nagajothi et al. (Nagajothi et al., 2022). The progression on the graph provides insight into the effectiveness of the strengthening system in enhancing the beam's load-carrying capacity and ductility.

The load-carrying capacity of the specimen CB, FF-50–1, FF-75–1, and FF-100–1 exhibited increased flexural capacity of 5.21%, 1.52%, 0.44%, and 3.86%, respectively, than the experimental results. Similarly, the ultimate load capacities of FF-50–2, FF-75–2, and FF-100–2 decreased to 1.55%, 4.54%, and 0.16%, respectively. Increasing the number of GFRCM layers improved the shear capacity of the retrofitted beams. The flexural capacity of the retrofitted beam decreased once it reached its ultimate load, signifying that the retrofitting effect was entirely nullified. This observation was also reported by Raoof et al. (Raoof et al., 2017).

4.1.3 Failure Modes

Figure 10 represents the failure of flexural-deficient retrofitted beams with GFRCM. The CB displayed significant flexural cracks at the mid-span and observed the crushing of the concrete at the top surface. Beams retrofitted with GFRCM demonstrated a slightly increased failure load owing to the enlarged cross-sectional area. The specimen pre-cracked to 50% and strengthened with one and two layers observed the formation of flexural cracks at the soffit of the beam with matrix debonding. Debonding refers to the separation of the strengthening materials from the concrete substrate, often at the interface due to weak bonding. This indicates that the strengthening layers were unable to absorb the bending stresses, resulting in the separation of the matrix from the FRCM. The specimen FF-75–1 exhibited the flexural

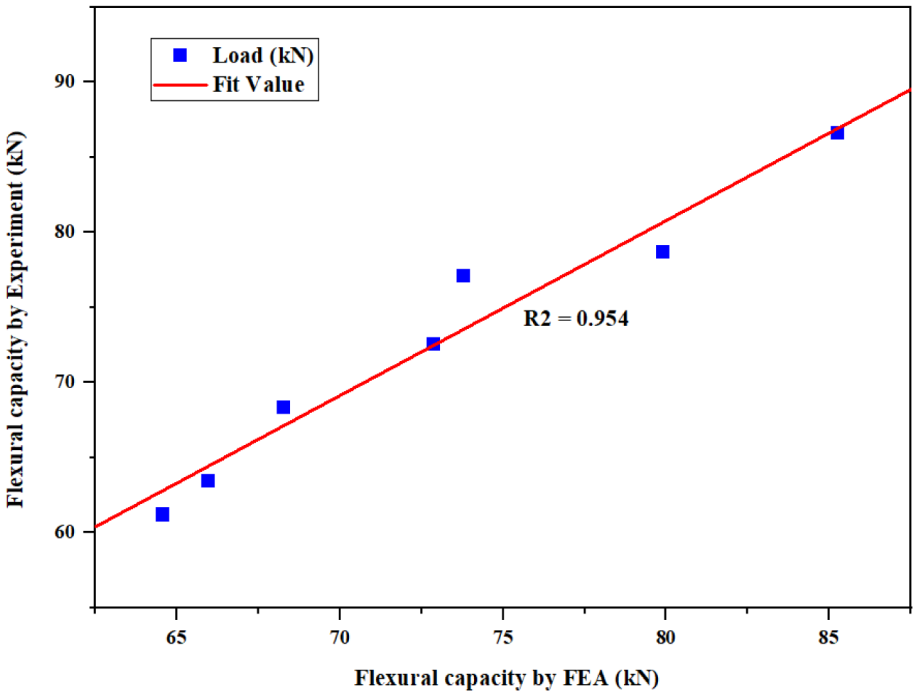

(a)

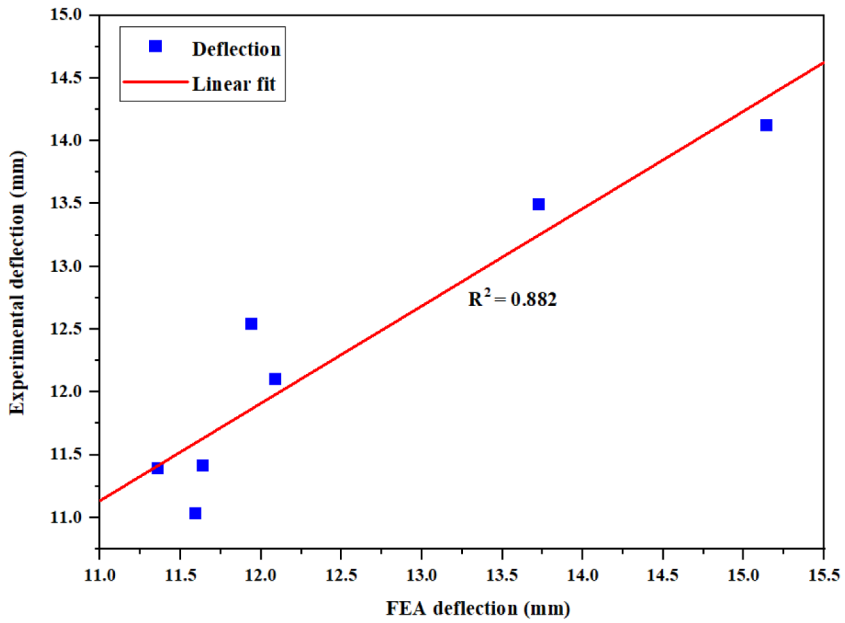

(b)

Fig. 8 Correlation between the experiemntal and FEA results. **a** Flexural capacity. **b** Deflection at the ultimate load

crack with matrix delamination due to an insufficient bond between the outer matrix and glass fabric, which was unable to resist the failure stresses. Delamination indicates the separation between layers within the composite material. This modes of failure observed by Elsanadedy et al. (2013), while the specimen FF-75–2 observed

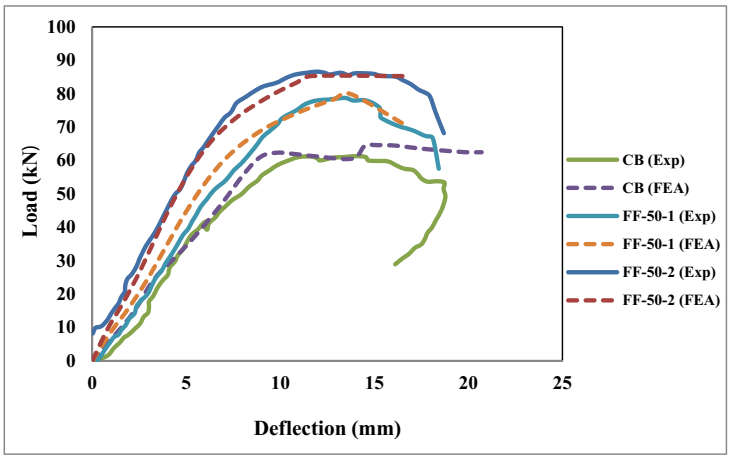

(a)

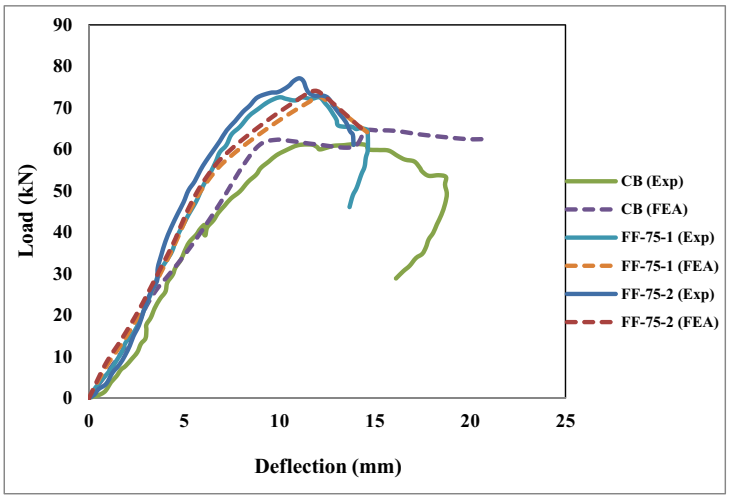

(b)

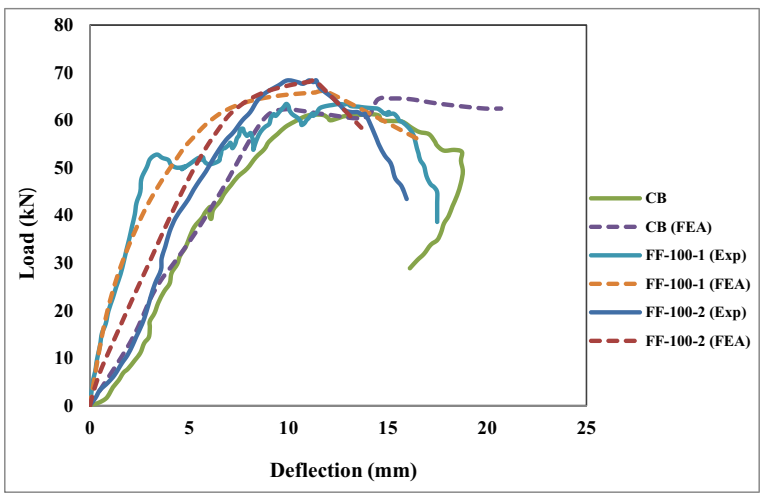

(c)

Fig. 9 Comparisons of FEA load–deflection curve with experimental results. **a** FF-50%. **b** FF-75%. **c** FF-100%

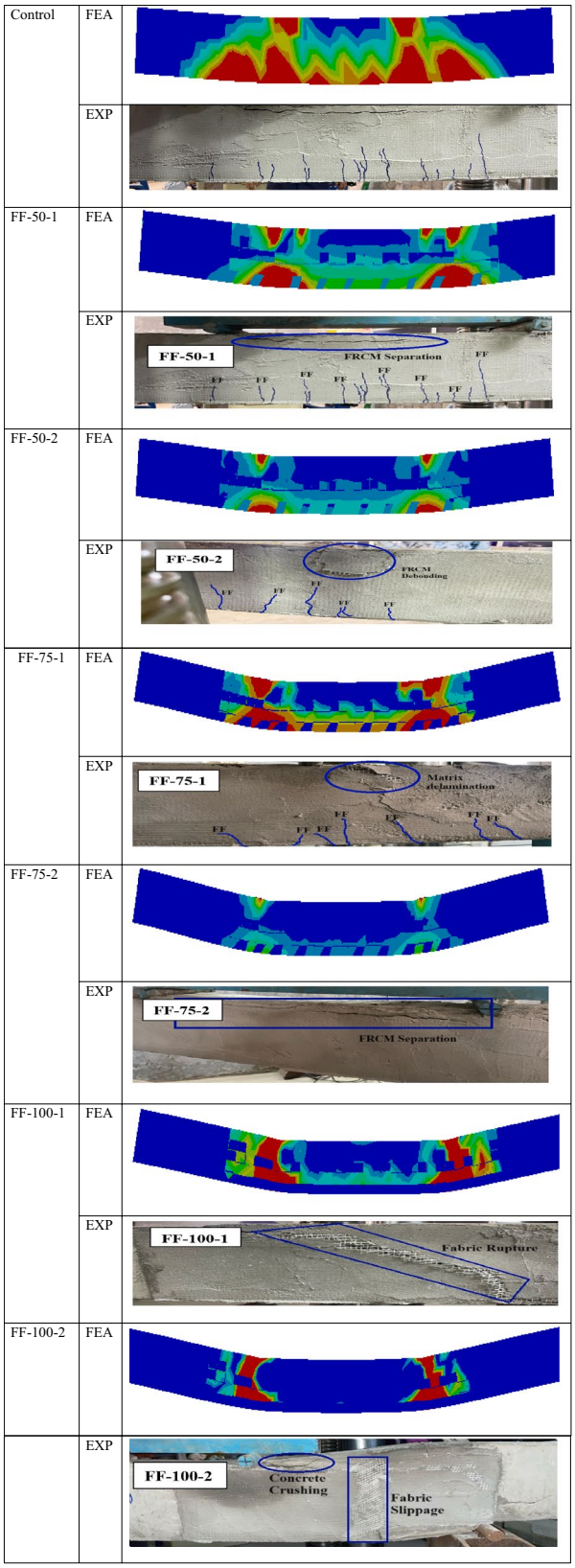

Fig. 10 Failures of flexural-deficient retrofitted beams

the delamination of FRCM. Similarly, the specimen pre-cracked to 100% observed the fabric rupture in FF-100–1, because the failure stresses exceeded the fabric's tensile strength, which led to rupture failure. Fabric slippage was observed in specimen FF-100–2 due to inadequate bonding between the fabric and matrix, causing the fabric to slide rather than fully resist the applied stresses (Jabr et al., 2017). Slippage refers to the relative movement of reinforcement inside the matrix due to poor anchorage, which reduces effective load transfer.

Pre-cracking the beam at different levels impacts the strength capacity and deformation properties of the strengthened beam. The beam pre-cracked to 50% and retrofitted with one and two layers showed an increase in load-carrying capacity of about 23.76% and 32.06% than CB Similar type of enhancements were observed by Awani et al. (2016) and Elghazy et al. (2017). This increased result proves the effective bond between the GFRCM and concrete substrate, which remains effective even after the pre-cracking. Similarly, the beam pre-cracked to 75% showed strength gains of approximately 12.84% and 14.26%, while the beam pre-cracked to 100% showed an increase in load of about 2.17% and 5.72%, indicating that severe pre-cracking greatly reduces the effectiveness of retrofitting. Giese et al. (2021) observed that beams strengthened with a cement binder experienced an 18% increase in load capacity with two layers, while three layers led to a 41.4% improvement compared to a single layer. Taie et al. (2024) retrofitted the RC beams with FRCM incorporating silica fume and cement binder, which resulted in a flexural moment increase between 23% and 37%. Moreover, the deformation of the retrofitted beam compared with CB decreased by 9.33% and 24.97% than CB, representing enhanced stiffness and reduced flexibility after strengthening, especially in beams with less pre-cracking. This highlights that retrofitting improves strength and reduces deformation, the extent of pre-cracking is critical in determining the effectiveness of the strengthening technique.

The finite-element analysis (FEA) results shown in Fig. 10 depict a detailed visualization of stress distribution in flexural-deficient RC beams strengthened with GFRCM. The unstrengthened control beam exhibits a high concentration of stress at the mid-span, with large red areas at the bottom surface, reflecting typical flexural behavior, where tensile stresses are concentrated at the bottom of the beam under load. After the beam is strengthened with GFRCM, a distinct change in the stress distribution is observed. For the beam FF-50–1, moderate stress intensities are observed, with red and orange zones focused around the mid-span, but these are less distinct than those seen in the control beam. Sivasuriyan et al. (2024) observed the similar failure zone pattern for

strengthened RC beams. This indicates that the GFRCM has begun to efficiently lessen the concentration of tensile stress, spreading it over a larger region. In FF-50–2, the stress distribution shows considerable improvement, with only isolated high-stress area at the bottom, showing that the GFRCM's ability to control crack propagation and enhance flexural strength under minimal pre-crack conditions.

4.2 Shear-Deficient Beams Retrofitted with GFRCM

The maximum load-carrying capacity of the shear-deficient retrofitted beam surpassed than CB. The specimens SF-50–1, SF-75–1, and SF-100–1, strengthened with single layers attained a maximum load of 61.53 kN, 56.06 kN, and 47.495 kN, respectively, with mid-span deflection of 12.5 mm, 9.84 mm, and 14.89 mm. The specimens SF-50–2, SF-75–2, and SF-100–2 failed at 73.49 kN, 65.65 kN, and 54.28 kN with deflection of 9.31 mm, 10 mm, and 12.70 mm. The specimen SF-75–1 shows an 8.39% decrease in load value compared to the CB, likely due to insufficient bonding with a concrete substrate, which affected the retrofitting effectiveness. The specimen pre-cracked to 100% showed a reduction in load by 22.39% with single wrapping, and 11.31% with double wrapping. The reduced load values in the specimens SF-100–1 and SF-100–2 were due to existing cracks that weakened the RC beams, diminishing the effectiveness of the retrofitting.

4.2.1 Comparison of FEA Result with Experiment Result

Table 8 presents the load-carrying capacity and deflection of the retrofitted beams from numerical and experimental analyses. Table 8 also provides the ratio of FE to experimental load-carrying capacity and displacements of the retrofitted beams. The shear capacity of the retrofitted beam ranges from 0.90 to 1.06, with a correlation of 0.878, while the deflection varies between 0.93 and 1.08 with a correlation coefficient of 0.948, as shown in Fig. 11. The load–deflection curve from both experimental and FE analysis are closely matched, reflecting a strong agreement for all beams. This strong agreement highlights the accuracy of the FE model in predicting the performance of the retrofitted beams. This result accurately validates the numerical analysis and represents the actual behaviour of retrofitted beams. Al-Salloum et al. (2012) validated that FEA provides an accurate representation of shear behavior and failure mechanisms, with the predicted load-carrying capacities exhibiting strong agreement with experimental data, falling within a range of 0.95 to 1.08. The study Tzoura and Triantafillou, (2016) also emphasizes the application of validated numerical modeling approaches to accurately assess the structural performance of TRM-strengthened elements.

4.2.2 Load–Deflection Curve

Figure 12 represents the load–deflection curve for the shear-deficient retrofitted beams obtained from experiment and FEA. All retrofitted beams exhibited load–deflection curves with tri-linear behavior, indicating that the stiffness of the beam varies after the development of shear cracks. Initially, the graph shows a linear increase in stiffness with minimum deflection. As the load increases, the curve remains nearly linear, representing a gradual reduction in deflection. After reaching the ultimate load, the deflection increases more rapidly due to failure modes, such as the development of shear crack or matrix debonding. Beyond the ultimate load, the graph shows a significant drop in deformation with the debonding failure of the FRCM. The control beam (CB) initially shows linear elastic behavior and reaches a peak load of 61.2 kN, but its load-carrying capacity decreases due to shear failure. The FEA predicts a slightly higher peak load and more ductile behavior than experimental results. Retrofitted specimens SF-50–1, SF-50–2 and SF-75–2 showed an increased peak load of about 61.53 kN, 73.49 kN, and 65.66 kN, respectively, and showed a decrease in

Table 8 Load-carrying capacity and deflection of the shear-deficient retrofitted beam

Specimen	No. of layers	FEA		Experiment		P_A/P_E	δ_A/δ_E	Failure modes (Exp)
		Max. Load, P_A (kN)	Deflection, δ_A (mm)	Max. Load, P_E (kN)	Deflection, δ_E (mm)			
Control (CB)	–	64.565	15.14	61.2	14.12	0.95	0.93	Flexure Failure
SF-50%-1	1	59.41	12.185	61.533	12.5	1.04	1.03	Shear Failure
SF-50%-2	2	73.827	9.4845	73.487	9.31	1.00	0.98	Fabric Rupture + Slippage
SF-75%-1	1	55.736	9.9122	56.06	9.84	1.01	0.99	Fabric slippage + Debonding
SF-75%-2	2	62.196	9.2664	65.654	10	1.06	1.08	Shear + Fabric rupture
SF-100%-1	1	52.56	14.481	47.495	14.89	0.90	1.03	Shear + Fabric rupture
SF-100%-2	2	56.862	12.613	54.277	12.7	0.95	1.01	Shear Failure

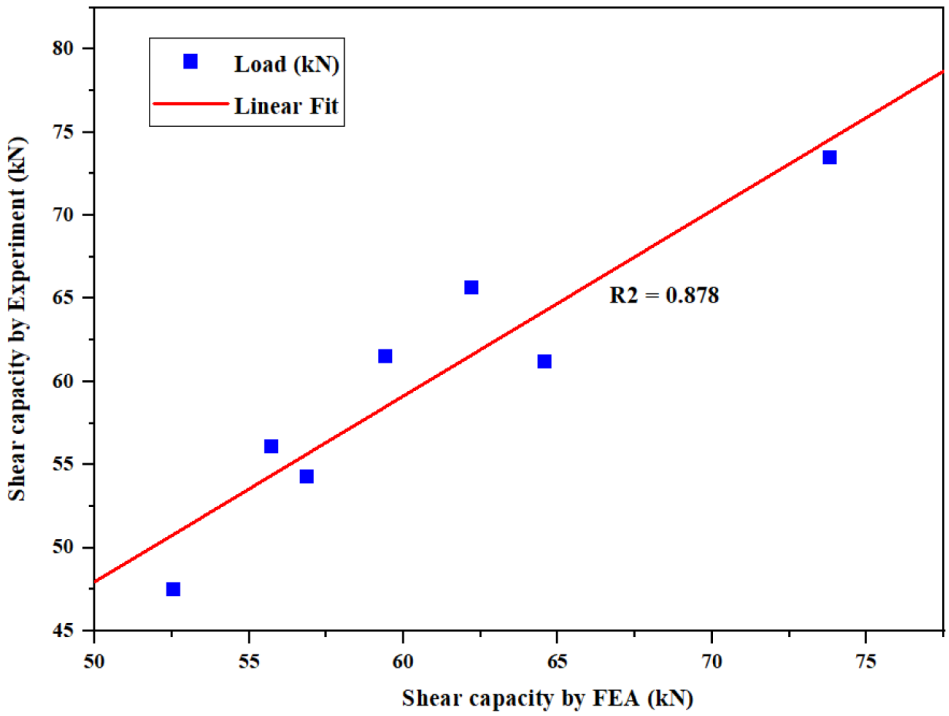

(a)

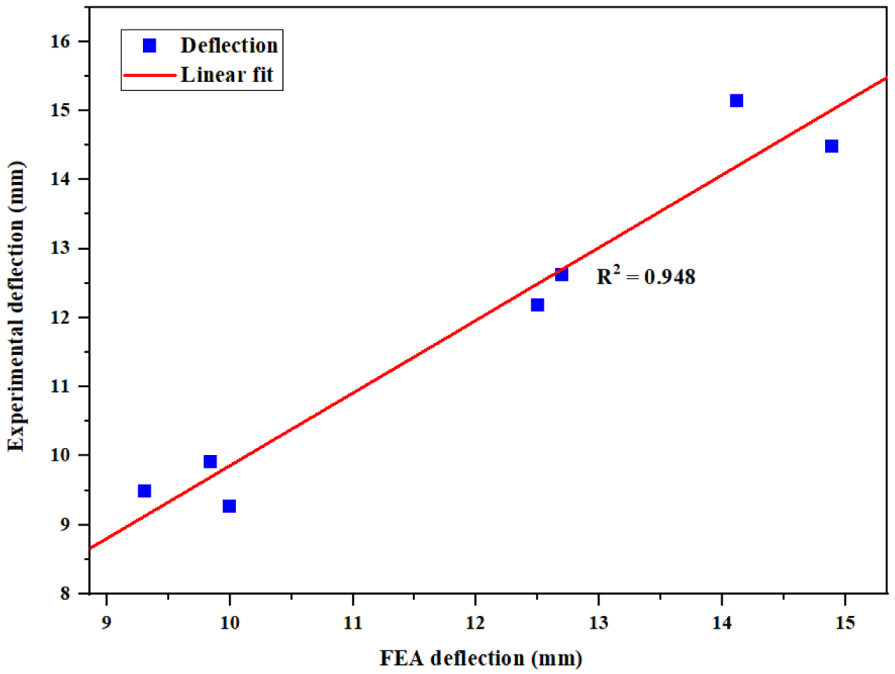

(b)

Fig. 11 Correlation between the experimental and FEA results. **a** Shear capacity. **b** Deflection at the ultimate load

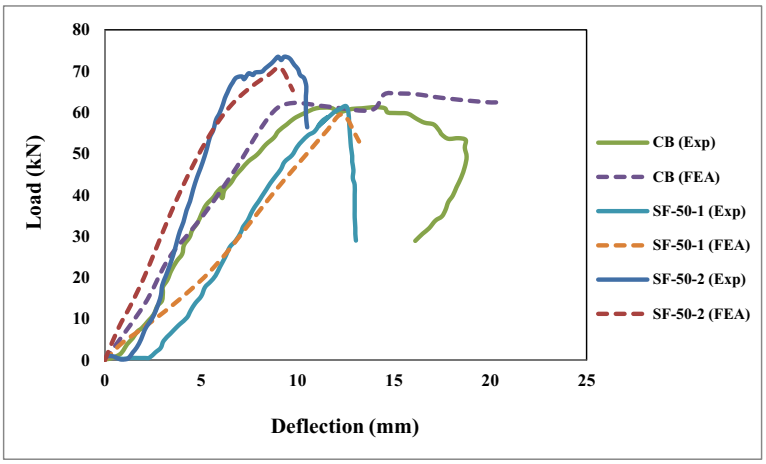

(a)

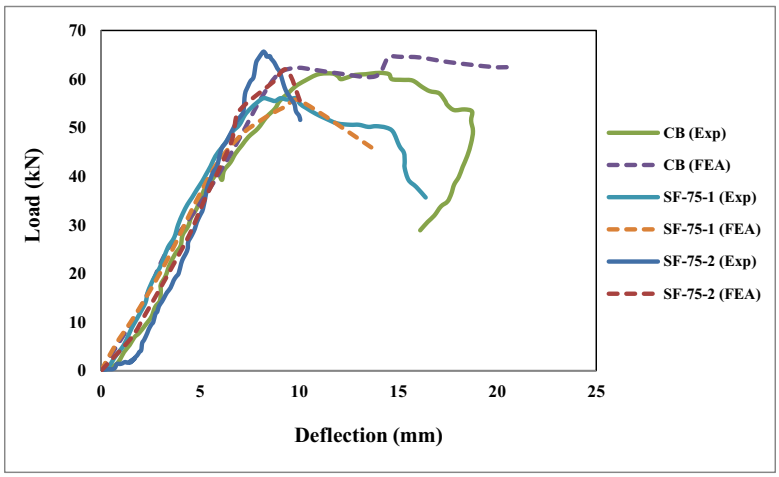

(b)

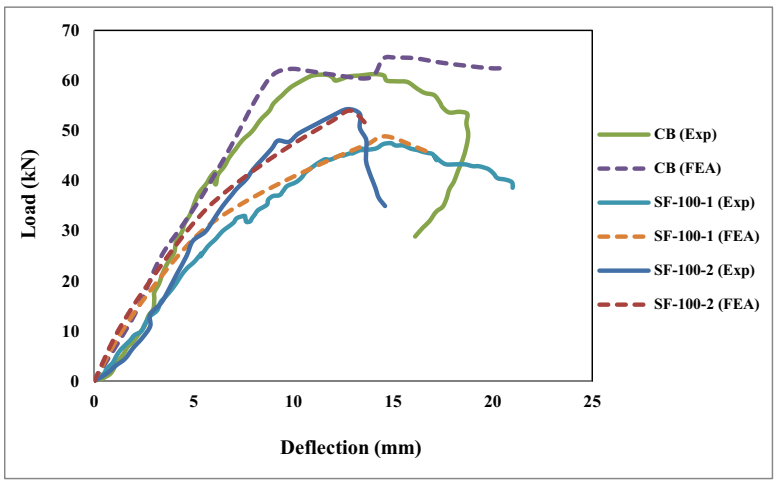

(c)

Fig. 12 Comparisons of FEA load–deflection curve with experimental results. **a** SF-50%. **b** SF-75%. **c** SF-100%

load after reaching the peak load due to shear cracks. The FEA models correlate with the experimental results, but predict slightly lower ultimate loads and declines in post-peak behaviour for the specimens SF-50–1, SF-100–1, and SF-100–2. Mercedes et al. (2021) also observed this reduction in their investigations.

The load-carrying capacity of CB, SF-50–2, SF-100–1, and SF-100–2 increased by 5.21%, 0.46%, 9.64%, and 4.55%, respectively, compared to experimental results. This improvement can be attributed to enhanced reinforcement, better bonding, and optimized strengthening methods. Moreover, accurate FE modelling likely contributed to these observed improvements than experimental results. The shear capacities of SF-50–1, SF-75–1, and SF-75–2, are decreased by 3.57%, 0.58%, and 5.56%, respectively, and this reduction may be due to pre-existing damage impacting the retrofitting applications. Moreover, the enhanced performance observed in the results can be attributed to the precision of FEM, which effectively simulates ideal boundary conditions and material behavior, thereby minimizing the inconsistencies commonly found in experimental testing.

4.2.3 Failure Modes

The retrofitted shear-deficient beam shows a visible shear cracks, as shown in Fig. 13, and also observed the less damage in the compressive zone. At diagonal cracks, transverse yarns in shorter bond lengths were completely ripped out, whereas longer bond lengths failed due to tensile stress. The beam pre-cracked to 50% shows many flexural cracks when compared to beam pre-cracked to 75% and 100%. The growth of shear cracks in the retrofitted beam caused rupture and slippage failure, ultimately leading to debonding failure, as reported by Ombres et al. (Ombres, 2015). In the specimens SF-50–1, SF-75–2, and SF-100–1, shears cracks developed in the shear area and they were accompanied by shear rupture with matrix debonding failures. (Guo et al. (2022) reported comparable failure patterns in their study. These failures resulted in a substantial reduction in the load-carrying capacity of the retrofitted beams. The specimen SF-100–2 displayed shear failure along with delamination of the GFRCM, and also observed the concrete crushing at the loading points with shear cracking in the matrix interfaces. Yang et al. (2020) attributed this to insufficient adhesion with the fabric grids and the cement matrix. The specimens SF-50–2 and SF-75–1 showed flexural cracks, indicating high bending stresses and observed fabric rupture and slippage failure, reducing the effectiveness of the retrofitting. Alotaibi et al. (2024) mentioned that beams with one or two layers of fabric failed due to fabric rupture, fully utilizing the FRCM system.

The shear capacity of the retrofitted beam, pre-cracked to 50%, 75%, and 100% exhibited a decrease in load ranging from 3.67% to 18.59% than CB. The reduction in shear capacity is due to the weakening of the beam from initial cracks, which reduces its cross-sectional area. This damage disrupts the bond among the concrete substrate with the GFRCM, and changes the load distribution, resulting in reduced shear strength even with retrofitting. However, the specimen SF-50%-2 showed an increase in load of about 14.21%, indicating that the retrofitting was effective in enhancing the strength of the specimens. The deflection of the retrofitted specimens decreased from 4.35% to 38.79%. This variation in deflection needs to improve the beam stiffness.

The FEA results shown in Fig. 7.9 illustrate the stress distribution and failure zones in strengthened RC beams with GFRCM, subjected to various pre-racking levels. The FEA results for beam SF-50–1, a notable concentration of stress near the left support, highlighted in red colour, indicating the initiation of shear failure. As the level of pre-cracking increases, as observed in SF-50–2 and SF-75–2, the stress zones expand along the beam span, and areas of high stress intensity appear near mid-span and supports. The red and orange zones indicate critical stress areas that are likely associated with fabric rupture and matrix debonding. In SF-100–1 and SF-100–2, the fully pre-cracked beams, the stress intensity spreads more extensively and becomes more severe, with larger red zones indicating a substantial decline in the performance of the strengthening system (Parandaman and Jayaraman, 2014). Overall, the FEA results clearly show that as the level of pre-cracking increases, the stress concentration becomes more intense and is less effectively controlled by the FRCM, suggesting a gradual decrease in the performance of the strengthening system.

5 Conclusion

This study demonstrates that agro-industrial waste can serve as an effective and eco-friendly binder for FRP systems, contributing both to structural enhancement and sustainable construction practices. The successful application confirms the potential of waste-derived materials in advanced composite retrofitting solutions. A finite-element simulation was developed to analyze the performance of RC beams retrofitted in flexure and shear-deficient. The developed simulation was compared with test results from the experiment. Based on this study, the following conclusions were drawn.

- The non-linear finite-element analysis effectively predicted the load-carrying capacity and load–deflection behaviour of the experimentally tested specimen retrofitted with GFRCM.

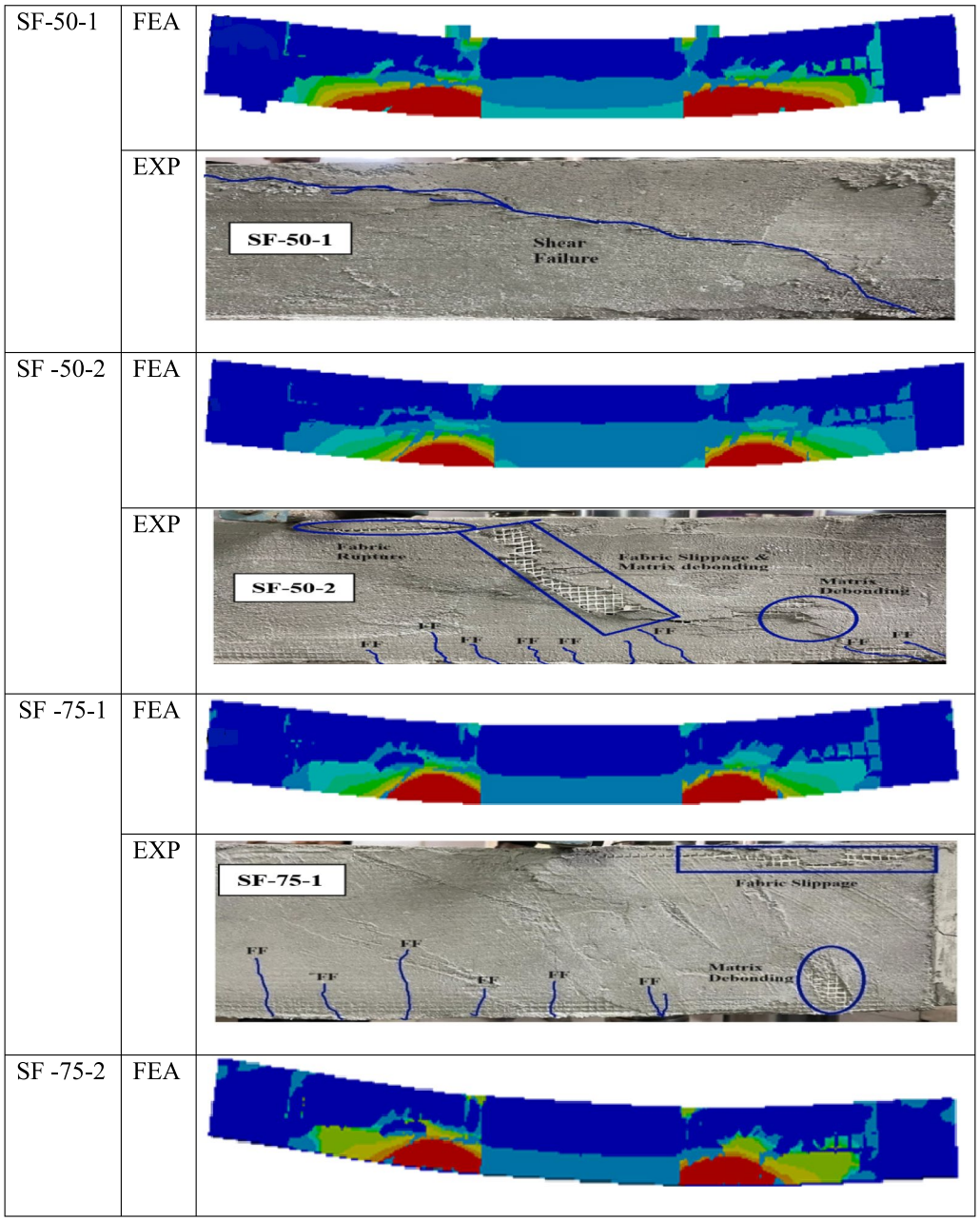

Fig. 13 Failures of shear-deficient retrofitted beams

- For flexural-deficient retrofitted beams, the specimens pre-cracked to 50% and retrofitted with one and two layers showed load increase of 23% and 32%, respectively. At 75% damage, the strength improved by 12% and 14%, while at 100% damage, the enhancements approximately 2% and 6%.
- Increasing the number of GFRCM layers enhances the flexural load-carrying capacity of the retrofitted beams but reduces their deflection.
- For shear-deficient retrofitted beams, the specimen pre-cracked to 50% exhibited an increased load capacity when retrofitted with two layers, but a decrease with only one layer. At 75% damage, the shear load dropped by 13.7% and 3.7% for one and two layers, respectively, while at 100% damage, the

shear strength further declined by 18.6% and 11.9%. This reduction is attributed to the influence of pre-existing damage on the effectiveness of the retrofitting.

- The failure modes of flexural-deficient retrofitted beams with single layer show flexural cracks along with matrix delamination, while the two layers exhibit wider flexural cracks with fabric slippage, concrete crushing, and fabric debonding.
- In shear-deficient retrofitted beams, a single layer exhibits fabric rupture with cracks extending toward the loading points, whereas two layers result in fabric slippage with matrix debonding.
- The error percentage between the finite-element analysis and the experimental results for load-carrying capacity and deflection of the retrofitted beams was within 10%.
- The FEA using ANSYS showed a strong correlation with the experimental results for the load–deflection curve of the retrofitted beams, with a correlation coefficient greater than 0.85.

5.1 Future Research

Future research is essential for enhancing the understanding of FRCM systems, especially in the following areas:

- Examining the performance of AR-GFRCM under varying environmental conditions, such as different humidity levels and temperatures, provides crucial insights into its durability and behavior in real-world applications.
- Moreover, evaluating its performance under long-term loading scenarios is essential for understanding its behavior over time.
- The application of this study could be expanded to include other structural components such as slabs**,** columns, and beam–column joints that have experienced deterioration
- The proposed strengthening technique could also be applied to damaged brick masonry**,** stone masonry, and timber structures.

These research areas are essential for addressing potential limitations and ensuring the reliable application of FRCM systems in diverse and challenging conditions.

Abbreviations

FRCM	Fabric-Reinforced Cementitious Matrix
RC	Reinforced Concrete
AR-GFRCM	Alkali-resistant glass fabric-reinforced cementitious matrix
PBO	Polyparaphenylene Benzobisoxazole
ACI	American Concrete Institute
OPC	Ordinary Portland cement
FF	Flexural-deficient retrofitted beam
SF	Shear-deficient retrofitted beams
CB	Control beam
P_u	Maximum load for retrofitted beam
P_c	Maximum load for control beam
FF	Flexural failure
D	Delamination
FR	Fabric rupture
CC	Concrete crushing
FD	Fabric Debonding
SF	Shear failure
FS	Fabric slippage

Acknowledgements
Authors would like to acknowledge the Management and Dean-School of Civil Engineering, Vellore Institute of Technology, Chennai, India for providing the necessary support to carry out this research.

Author Contributions
R. Kirthiga: conceptualization, methodology, investigation, writing—original draft and supervision. S. Elavenil: writing—review and editing, investigation and supervision.

Funding
Open access funding provided by Vellore Institute of Technology. No funding.

Availability of Data and Materials
The data will be available on request.

Declarations

Ethics Approval and Consent to Participate
The authors have complied with ethical standards.

Consent for Publication
Consent was obtained from all the authors for the publication of this manuscript.

Competing Interests
The authors declare no competing interests.

Received: 3 October 2024 Accepted: 26 June 2025
Published online: 10 September 2025

References

Al-Huri, M. A., Al-Osta, M. A., & Ahmad, S. (2022). Finite Element modelling of corrosion-damaged rc beams strengthened using the UHPC layers. *Materials*. https://doi.org/10.3390/ma15217606

Aljazaeri, Z. R., & Myers, J. J. (2016). Fatigue and flexural behaviour of reinforced concrete beams strengthened with a fibre reinforced cementitious matrix. *Journal of Composites for Construction, 21*(3), 128–134. https://doi.org/10.1061/(asce)cc.1943-5614.0000726

Alotaibi, S., Thermou, G., Hajirasouliha, I., & Guadagnini, M. (2024). Effect of textile density and number of layers on the flexural behaviour of RC beams strengthened with steel reinforced grout systems. *Construction and Building Materials*. https://doi.org/10.1016/j.conbuildmat.2024.136424

Al-Salloum, Y. A., Elsanadedy, H. M., Alsayed, S. H., & Iqbal, R. W. (2012). Experimental and numerical study for the shear strengthening of reinforced concrete beams using textile- reinforced mortar. *Journal of Composites for Construction, ASCE, 16*(1), 74–90. https://doi.org/10.1061/(ASCE)CC.1943-5614.0000239

Awani, O., El-Maaddawy, T., & El Refai, A. (2016). Numerical simulation and experimental testing of concrete beams strengthened in shear with fabric-reinforced cementitious matrix. *Journal of Composites for Construction, 20*(6), 04016056. https://doi.org/10.1061/(asce)cc.1943-5614.0000711

Azam, R., Soudki, K., West, J. S., & Noël, M. (2018). Shear strengthening of RC deep beams with cement-based composites. *Engineering Structures, 172*(2017), 929–937. https://doi.org/10.1016/j.engstruct.2018.06.085

Barhum, R., & Mechtcherine, V. (2012). Effect of short fibers on the behavior of textile reinforced concrete under tensile loading. *RILEM Bookseries, 2*, 487–494. https://doi.org/10.1007/978-94-007-2436-5_59

Chen, X., Yan, Z., Al-Nuaimi, N. A., & Xiong, Z. (2023). Compressive behaviour of concrete column confined with basalt textile reinforced ECC. *Lecture Notes in Civil Engineering, 284*(June), 389–401. https://doi.org/10.1007/978-3-031-12011-4_30

ACI Committee 549.4R-13. (2013). *Guide to Design and Construction of Externally Bonded Fabric-Reinforced Cementitous Matrix (FRCM) Systems for Repair and Strengthening Concrete Structures. ACI*.

D'Ambrisi, A., & Focacci, F. (2011). Flexural strengthening of RC beams with cement-based composites. *Journal of Composites for Construction, 15*(5), 707–720. https://doi.org/10.1061/(asce)cc.1943-5614.0000218

Dong, Z., Deng, M., Zhang, Y., Zhang, C., & Ma, P. (2020). Out-of-plane strengthening of unreinforced masonry walls using textile reinforced mortar added short polyvinyl alcohol fibers. *Construction and Building Materials, 260*, 119910.

Donnini, J., Corinaldesi, V., & Nanni, A. (2016a). Mechanical properties of FRCM using carbon fabrics with different coating treatments. *Composite Part B, 88*, 220–228. https://doi.org/10.1016/j.compositesb.2015.11.012

Donnini, J., Corinaldesi, V., & Nanni, A. (2016b). Mechanical properties of FRCM using carbon fabrics with different coating treatments. *Composites Part B: Engineering, 88*, 220–228. https://doi.org/10.1016/j.compositesb.2015.11.012

Donnini, J., De Caso y Basalo, F., Corinaldesi, V., Lancioni, G., & Nanni, A. (2017). Fabric-reinforced cementitious matrix behavior at high-temperature: Experimental and numerical results. *Composites Part b: Engineering, 108*, 108–121. https://doi.org/10.1016/j.compositesb.2016.10.004

Ebead, U., Shrestha, K. C., Afzal, M. S., El Refai, A., & Nanni, A. (2017). Effectiveness of fabric-reinforced cementitious matrix in strengthening reinforced concrete beams. *Journal of Composites for Construction, 21*(2), 04016084. https://doi.org/10.1061/(asce)cc.1943-5614.0000741

Ebead, U., & Younis, A. (2019). Pull-off characterization of FRCM/Concrete interface. *Composites Part b: Engineering, 165*(2019), 545–553. https://doi.org/10.1016/j.compositesb.2019.02.025

Elghazy, M., El Refai, A., Ebead, U., & Nanni, A. (2017). Effect of corrosion damage on the flexural performance of RC beams strengthened with FRCM composites. *Composite Structures, 180*, 994–1006. https://doi.org/10.1016/j.compstruct.2017.08.069

El-Maaddawy, T., & El Refai, A. (2016). Innovative repair of severely corroded t-beams using fabric-reinforced cementitious matrix. *Journal of Composites for Construction, 20*(3), 04015073. https://doi.org/10.1061/(asce)cc.1943-5614.0000641

Elsanadedy, H. M., Abbas, H., Almusallam, T. H., & Al-Salloum, Y. A. (2019). Organic versus inorganic matrix composites for bond-critical strengthening applications of RC structures–State-of-the-art review. *Composites Part b: Engineering*. https://doi.org/10.1016/j.compositesb.2019.106947

Elsanadedy, H. M., Almusallam, T. H., Alsayed, S. H., & Al-Salloum, Y. A. (2013). Flexural strengthening of RC beams using textile reinforced mortar–experimental and numerical study. *Composite Structures, 97*, 40–55. https://doi.org/10.1016/j.compstruct.2012.09.053

El-Sherif, H. E., Wakjira, T. G., & Ebead, U. (2020). Flexural strengthening of reinforced concrete beams using hybrid near-surface embedded/externally bonded fabric-reinforced cementitious matrix. *Construction and Building Materials*. https://doi.org/10.1016/j.conbuildmat.2019.117748

Giese, A. C. H., Giese, D. N., Dutra, V. F. P., & Filho, L. C. P. D. S. (2021). Flexural behavior of RC beams strengthened with textile reinforced concrete. *Journal of Building Engineering*. https://doi.org/10.1007/978-3-031-05509-6_18

Grande, E., & Milani, G. (2018). Interface Modeling approach for the study of the bond behavior of FRCM strengthening systems. *Composites Part B: Engineeringb, 141*, 221–233. https://doi.org/10.1016/j.compositesb.2017.12.052.This

Guo, L. D., Chen, M., Li, H., Ma, R., & Xiangkun Zhang, Y. (2022). Experimental study on pre-damaged RC beams shear-strengthened with textile-reinforced mortar (TRM). *Engineering Solid Mechanics, 256*, 0141–0296. https://doi.org/10.1016/j.engstrut.2022.113956

Hao, R., Lin, W., Al-Nuaimi, N. A., Hawileh, R. A., Abdalla, J. A., & Elshafie, M. Z. E. B. (2022). Short-term and long-term behavior of RC beams strengthened by galvanized steel mesh laminate. *Construction and Building Materials*. https://doi.org/10.1016/j.conbuildmat.2022.127763

Hassan, N. Z., Sherif, A. G., & Zamarawy, A. H. (2017). Finite element analysis of reinforced concrete beams with opening strengthened using FRP. *Ain Shams Engineering Journal, 8*(4), 531–537. https://doi.org/10.1016/j.asej.2015.10.011

IS: 14858:2000. (2000). Compression Testing Machine used for Testing of Concrete and Mortar-Requirements. *Bureau of Indian Standards*.

Jabr, A., El-Ragaby, A., & Ghrib, F. (2017). Effect of the fiber type and axial stiffness of FRCM on the flexural strengthening of RC beams. *Fibers*. https://doi.org/10.3390/fib5010002

Jawdhari, A., Adheem, A. H., & Kadhim, M. M. A. (2020). Parametric 3D finite element analysis of FRCM-confined RC columns under eccentric loading. *Engineering Structures, 212*(2019), 110504. https://doi.org/10.1016/j.engstruct.2020.110504

Kalyani, G., & Pannirselvam, N. (2023). Experimental and numerical investigations on RC beams flexurally strengthened utilizing hybrid FRP sheets. *Results in Engineering*. https://doi.org/10.1016/j.rineng.2023.101337

Katsamakas, A. A., Papanikolaou, V. K., & Thermou, G. E. (2021). A FEM-based model to study the behavior of SRG-strengthened R/C beams. *Composite Structures, 266*(2020), 1–12. https://doi.org/10.1016/j.compstruct.2021.113796

Kirthiga, R., & Elavenil, S. (2022). A review on using inorganic binders in fiber reinforced polymer at different conditions to strengthen reinforced concrete beams. *Construction and Building Materials*. https://doi.org/10.1016/j.conbuildmat.2022.129054

Kirthiga, R., & Elavenil, S. (2023). Potential utilization of sugarcane bagasse ash in cementitious composites for developing inorganic binder. *Ain Shams Engineering Journal*. https://doi.org/10.1016/j.asej.2023.102560

Kirthiga, R., & Elavenil, S. (2024). Experimental and analytical study of tensile and bond performances of glass fabric reinforced cementitious matrix for retrofit applications on concrete surfaces. *International Journal of Civil Engineering*. https://doi.org/10.1007/s40999-024-01035-3

Koutas, L. N., Tetta, Z., Bournas, D. A., & Triantafillou, T. C. (2019). Strengthening of concrete structures with textile reinforced mortars: state-of-the-art review. *Journal of Composites for Construction, 23*(1), 1–20. https://doi.org/10.1061/(asce)cc.1943-5614.0000882

Mahmoud, A. M. (2016). Finite element modeling of steel concrete beam considering double composite action. *Ain Shams Engineering Journal, 7*(1), 73–88. https://doi.org/10.1016/j.asej.2015.03.012

Mercedes, L., Escrig, C., Bernat-Masó, E., & Gil, L. (2021). Analytical approach and numerical simulation of reinforced concrete beams strengthened with different frcm systems. *Materials*. https://doi.org/10.3390/ma14081857

Mohan, A., & Madhavi, T. C. (2024). Flexural behavior of warp knitted textile reinforced concrete impregnated with cementitious binder. *Case Studies in Construction Materials*. https://doi.org/10.1016/j.cscm.2024.e02884

Nagajothi, S., Elavenil, S., Angalaeswari, S., Natrayan, L., & Paramasivam, P. (2022). Cracking behaviour of alkali-activated aluminosilicate beams reinforced with glass and basalt fibre-reinforced polymer bars under cyclic load. *International Journal of Polymer Science*. https://doi.org/10.1155/2022/6762449

Natraj, K., Kirthiga, R., & Elavenil, S. (2023). Structural performance of RCC building and strengthening the structural members with CFRP. *Materials Today: Proceedings, 84*, 24–32. https://doi.org/10.1016/j.matpr.2023.04.304

Ombres, L. (2011). Flexural analysis of reinforced concrete beams strengthened with a cement based high strength composite material. *Composite Structures, 94*(1), 143–155. https://doi.org/10.1016/j.compstruct.2011.07.008

Ombres, L. (2015). Structural performances of reinforced concrete beams strengthened in shear with a cement based fiber composite material. *Composite Structures, 122*(2015), 316–329. https://doi.org/10.1016/j.compstruct.2014.11.059

Ombres, L., & Verre, S. (2019). Flexural strengthening of rc beams with steel-reinforced grout: experimental and numerical investigation. *Journal of Composites for Construction, 23*(5), 1–13. https://doi.org/10.1061/(asce)cc.1943-5614.0000960

Ombres, L., & Verre, S. (2021). Shear strengthening of reinforced concrete beams with SRG (Steel Reinforced Grout) composites: Experimental investigation and modelling. *Journal of Building Engineering*. https://doi.org/10.1016/j.jobe.2021.103047

Omran, H. Y., & El-Hacha, R. (2012). Nonlinear 3D finite element modeling of RC beams strengthened with prestressed NSM-CFRP strips. *Construction and Building Materials, 31*, 74–85. https://doi.org/10.1016/j.conbuildmat.2011.12.054

Ramezani, A., & Esfahani, M. R. (2023). Shear strengthening of RC beams using FRCM system made with industrial wastes. *Structures, 48*(January), 1833–1847. https://doi.org/10.1016/j.istruc.2023.01.078

Raoof, S. M., Koutas, L. N., & Bournas, D. A. (2017). Textile-reinforced mortar (TRM) versus fibre-reinforced polymers (FRP) in flexural strengthening of RC beams. *Construction and Building Materials, 151*, 279–291. https://doi.org/10.1016/j.conbuildmat.2017.05.023

Revanna, N., & Moy, C. K. S. (2023). Numerical modelling of reinforced concrete flexural members strengthened using textile reinforced mortars. *Frontiers of Structural and Civil Engineering, 17*(4), 649–668. https://doi.org/10.1007/s11709-023-0919-4

Sagare, S. S., Kirthiga, R., & Elavenil, S. (2024). A state of art of review on strengthening of concrete structures using fabric reinforced cementitious matrix. *Research on Engineering Structures and Materials, 10*(3), 1–30. https://doi.org/10.17515/resm2024.133ma1226rv

Sasikumar, P., & Candassamy, K. (2024). Strengthening of flexural behavior of reinforced concrete beams by using hybrid fibers: Experimental and analytical study. *Revista de la construccion, 23*(2), 354–373. https://doi.org/10.7764/RDLC.23.2.354

Si Larbi, A., Agbossou, A., & Hamelin, P. (2013). Experimental and numerical investigations about textile-reinforced concrete and hybrid solutions for repairing and/or strengthening reinforced concrete beams. *Composite Structures, 99*, 152–162. https://doi.org/10.1016/j.compstruct.2012.12.005

Sivasuriyan, A., Vijayan, D. S., Sankaran, N., & Parthiban, D. (2024). Finite element analysis of RC beams using static experimental data to predict static and dynamic behaviors. *Scientific Reports, 14*(1), 31238. https://doi.org/10.1038/s41598-024-82537-x

Song, S., Deng, M., Zhang, M., Guo, L., Dong, Z., & Li, P. (2023). Flexural strengthening of reinforced concrete beams using textile-reinforced mortar improved with short PVA fibers. *Structures, 56*(April), Article 104824. https://doi.org/10.1016/j.istruc.2023.07.014

Sucharda, O. (2020). Identification of fracture mechanic properties of concrete and analysis of shear capacity of reinforced concrete beams without transverse reinforcement. *Materials, 13*(12), 1–22. https://doi.org/10.3390/ma13122788

Taie, B., Mandor, A., & El Refai, A. (2024). Experimental and numerical investigation of two–span RC beams strengthened with fiber–reinforced cementitious matrix (FRCM). *Engineering Structures*. https://doi.org/10.1016/j.engstruct.2023.117246

Talaat, M., Yehia, E., Mazek, S. A., Genidi, M. M. M., & Sherif, A. G. (2022). Finite element analysis of RC buildings subjected to blast loading. *Ain Shams Engineering Journal*. https://doi.org/10.1016/j.asej.2021.101689

Tetta, Z. C., Koutas, L. N., & Bournas, D. A. (2016). Shear strengthening of full-scale RC T-beams using textile-reinforced mortar and textile-based anchors. *Composites Part B: Engineering, 95*, 225–239. https://doi.org/10.1016/j.compositesb.2016.03.076

Truong, B. T., Si Larbi, A., & Limam, A. (2016). Numerical modelling of reinforced concrete beams repaired by TRC composites. *Composite Structures, 152*, 779–790. https://doi.org/10.1016/j.compstruct.2016.05.071

Tzoura, E., & Triantafillou, T. C. (2016). Shear strengthening of reinforced concrete T-beams under cyclic loading with TRM or FRP jackets. *Materials and Structures/materiaux Et Constructions, 49*(1–2), 17–28. https://doi.org/10.1617/s11527-014-0470-9

Wakjira, T. G., & Ebead, U. (2018). Hybrid NSE/EB technique for shear strengthening of reinforced concrete beams using FRCM: experimental study. *Construction and Building Materials, 164*, 164–177. https://doi.org/10.1016/j.conbuildmat.2017.12.224

Wei, B., Xiongjun, H., Weiwei, C. T. W., & Jia, H. (2025). Finite element analysis of ductility and flexural capacity of FRP and steel bars hybrid reinforced concrete beams. *Structural Concre, 2023*, 952–971. https://doi.org/10.1002/suco.202301066

Yang, X., Gao, W. Y., Dai, J. G., & Lu, Z. D. (2020). Shear strengthening of RC beams with FRP grid-reinforced ECC matrix. *Composite Structures, 241*, Article 112120. https://doi.org/10.1016/j.compstruct.2020.112120

Yin, S.-P., Sheng, J., Wang, X.-X., & Li, S.-G. (2016). Experimental Investigations of the Bending Fatigue Performance of TRC-Strengthened RC Beams in Conventional and Aggressive Chlorate Environments. *Journal of Composites for Construction, 20*(2), 04015051. https://doi.org/10.1061/(asce)cc.1943-5614.0000617

Zeng, L., Li, L. J., & Liu, F. (2017). Experimental study on fibre-reinforced cementitious matrix confined concrete columns under axial compression. *Kemija u Industriji/journal of Chemists and Chemical Engineers, 66*(3–4), 165–172. https://doi.org/10.15255/KUI.2016.039

Zhang, M., & Deng, M. (2022). Fabric-to-cementitious matrix bond behavior in carbon fabric reinforced cementitious matrix (FRCM) composites with added short fibers. *Composite Structures*. https://doi.org/10.1016/j.compstruct.2022.116173

Zreid, I., & Kaliske, M. (2018). A gradient enhanced plasticity–damage microplane model for concrete. *Computational Mechanics, 62*(5), 1239–1257. https://doi.org/10.1007/s00466-018-1561-1

Publisher's Note

R. Kirthiga is a research associate at Vellore Institute of Technology, Chennai, and is currently pursuing her Ph.D. Her research focuses on the strengthening of concrete structural members. She holds a B.E. in civil engineering from Anna University and a postgraduate degree from SASTRA University.

Dr. S. Elavenil is the professor in the Department of Civil Engineering at Vellore Institute of Technology, Chennai. She holds a Ph.D. from Anna University and has over 30 years of teaching experience. Her research expertise includes impact loading and structural dynamics, and she has authored four books in structural engineering. She has received several honors, including the VIVA Lifetime Achievement Award and the Women's Women Award in 2016.